Interpretation of hydraulic rock types with resistivity logs in Tertiary deepwater turbidite reservoirs: Pore-scale modeling verified with field observations in the Gulf of Mexico, USA

Chicheng Xu[1], Carlos Torres-Verdín[2], and Shuang Gao[2]

Abstract

Well-log-based hydraulic rock typing is critical in deepwater reservoir description and modeling. Resistivity logs are often used for hydraulic rock typing due to their high sensitivity to rock textural attributes such as porosity and tortuosity. However, resistivity logs measured at different water saturation conditions need to be cautiously used for hydraulic rock typing because, by definition, the properties of hydraulic rock types (HRT) are independent of fluid saturation. We compare theoretical models of electrical and hydraulic conductivity of clastic rocks exhibiting different pore-size distributions and originating from different sedimentary grain sizes. When rocks exhibiting similar porosity ranges are fully saturated with high-salinity water, hydraulic conductivity is dominantly controlled by characteristic pore size while electrical conductivity is only marginally affected by the characteristic pore size. As a result, rock types with similar porosity but different characteristic pore sizes cannot be effectively differentiated with resistivity logs in a water-bearing zone. In a hydrocarbon-bearing zone at irreducible water saturation, capillary pressure gives rise to specific desaturation behaviors in different rock types during hydrocarbon migration, thereby causing differentiable resistivity log attributes that are suitable for classifying HRT. Core data and well logs acquired from a deep-drilling exploration well penetrating Tertiary turbidite oil reservoirs in the Gulf of Mexico, verify that inclusion of resistivity logs in the rock classification workflow can significantly improve the accuracy of hydraulic rock typing in zones at irreducible water saturation. Classification results exhibit a good agreement with those obtained from nuclear magnetic resonance logs, but have relatively lower vertical resolution. The detected and ranked HRT exhibit different grain-size distributions, which provide useful information for sedimentary facies analysis.

Introduction

Electrical and hydraulic conductivity are two important physical properties closely related to the pore network system (Archie, 1942; Wildenschild et al., 2000; Revil and Leroy, 2001; Revil, 2013). Hydraulic conductivity is critical in fluid flow modeling of subsurface aquifers and hydrocarbon reservoirs. In most Tertiary turbidite reservoirs, hydraulic conductivity is mainly controlled by sedimentary grain sizes (Detmer, 1995; Evans et al., 1997; Revil and Cathles, 1999), which provide a connection between hydraulic rock types (HRT) and sedimentary facies. Therefore, accurate determination of HRT has great potential in assisting sedimentary facies interpretation and subsurface reservoir modeling. Among all types of borehole geophysical logs, nuclear magnetic resonance (NMR), and wireline formation testing provide the best estimate of hydraulic conductivity (Allen et al., 2000; Schlumberger, 2006). However, NMR logs and formation testing are often limited in their coverage of vertical reservoir columns. Resistivity logs, which are routinely acquired in almost every well, are often used for estimating hydraulic conductivity and classifying HRT in wells without NMR logs (Asquith and Gibson, 1982; Xu and Torres-Verdín, 2012; Xu et al., 2013a). To substitute NMR logs with resistivity logs for accurate hydraulic rock typing, the relation between rock electrical and hydraulic properties at different reservoir conditions (water salinity, water saturation, and capillary pressure) needs to be investigated. In this paper, we first use well-established theoretical models from existing literature to study the sensitivity of resistivity logs to different HRT in water- and hydrocarbon-bearing zones. We then develop pore-scale models to understand the relation between hydraulic properties

[1]Formerly The University of Texas at Austin, Petroleum & Geosystems Engineering Department, Texas, USA; presently BP America, Texas, USA. E-mail: Chicheng.Xu@bp.com.

[2]The University of Texas at Austin, Petroleum & Geosystems Engineering Department, Texas, USA. E-mail: cverdin@mail.utexas.edu; rebecca.shuang@gmail.com.

Manuscript received by the Editor 14 March 2013; revised manuscript received 3 August 2013; published online 16 October 2013. This paper appears in *Interpretation*, Vol. 1, No. 2 (November 2013); p. T177–T185, 12 FIGS., 3 TABLES.

http://dx.doi.org/10.1190/INT-2013-0037.1.

and resistivity measurements and to verify interpretations of HRT with field data acquired from a Miocene turbidite oil reservoir in the Gulf of Mexico, USA. Results can be useful to guide deepwater hydrocarbon exploration and production by reducing uncertainty associated with sedimentary facies interpretation (Xu et al., 2013b, 2013c) and subsurface reservoir modeling.

Conductivity models: Electrical versus hydraulic

Johnson et al. (1986a) and Pride (1994) have developed a model for quantifying the electrical conductivity (σ_t) of a 100% water-saturated rock based on a volume-averaging approach

$$\sigma_t = \frac{1}{F}\left[\sigma_w + \frac{2}{\Lambda}\Sigma_s\right], \tag{1}$$

where σ_w is electrical conductivity of water, Σ_s denotes specific surface conductivity associated with the diffuse part of the electrical double layer and the Stern layer (Revil and Glover, 1998; Bolève et al., 2007), and Λ is dynamic characteristic pore size defined by Johnson et al. (1986b). The formation factor (F) of a porous rock is defined by Walsh and Brace (1984) as

$$F = \frac{\tau^2}{\phi}, \tag{2}$$

where τ denotes tortuosity of the fluid or electrical current flow path and ϕ is interconnected porosity. The single-phase hydraulic conductivity (k) of a rock is quantified as (Johnson et al., 1986a)

$$k = \frac{\Lambda^2}{8F}. \tag{3}$$

Revil (2013) has extended equation 1 to estimate the electrical conductivity of a partially saturated rock with scaling laws

$$\sigma_t = \frac{1}{FS_w^{-n}}\left[\sigma_w + \frac{2}{\Lambda S_w}\Sigma_s\right], \tag{4}$$

where S_w is water saturation, and n is saturation exponent. If the surface conductivity term in equation 4 becomes negligible, equation 4 simplifies to Archie's (1942) equation. Electrical and hydraulic conductivity are inversely proportional to formation factor and both are functions of the characteristic pore size. However, electrical conductivity and hydraulic conductivity have very different sensitivity to the characteristic pore size. Furthermore, their relations are highly dependent on the saturating fluids.

Sensitivity of resistivity to HRT in a water-bearing zone

Figure 1a shows the relation between the electrical conductivity and the characteristic pore size, Λ, in 100% water-saturated rocks with different water salinity (assuming constant porosity and formation factor).

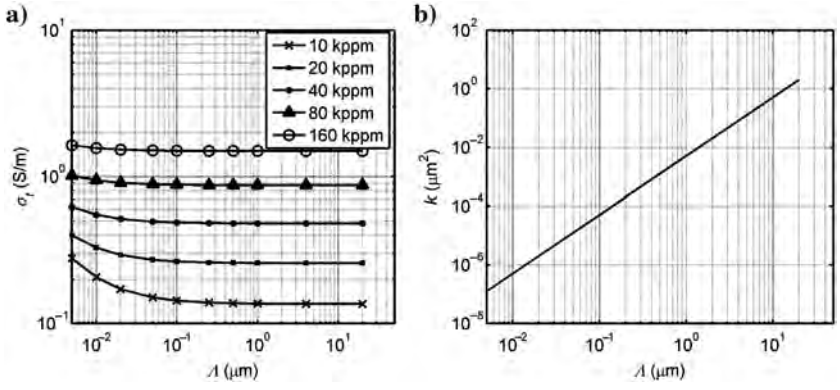

Figure 1. Theoretical calculation of the electrical and hydraulic conductivity as functions of characteristic pore sizes in fully water-saturated rocks ($\phi = 0.2$, $F = 25$, $\Sigma_s = 8.9 \times 10^{-9}$ S). (a) electrical conductivity versus characteristic pore size with different water salinity as indicated in equation 1; (b) hydraulic conductivity versus characteristic pore size as indicated in equation 3.

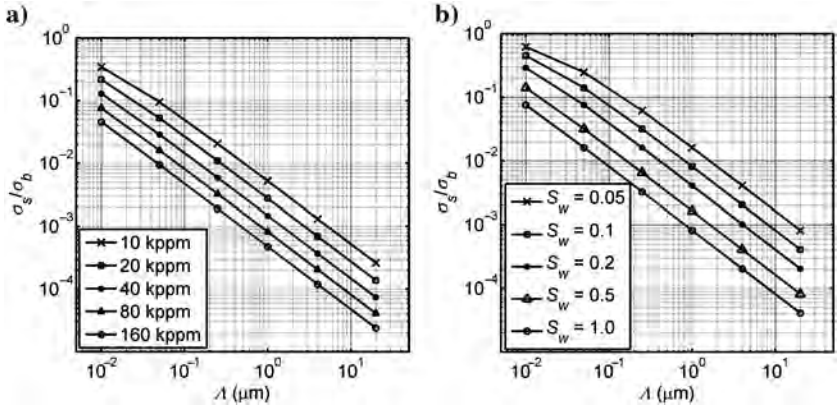

Figure 2. Theoretical calculation of the ratio between surface conductivity and bulk conductivity terms included in equation 4 as a function of characteristic pore size. (a) Fully water-saturated rock with different values of water salinity; (b) constant water salinity (80 kppm NaCl) with different values of water saturation.

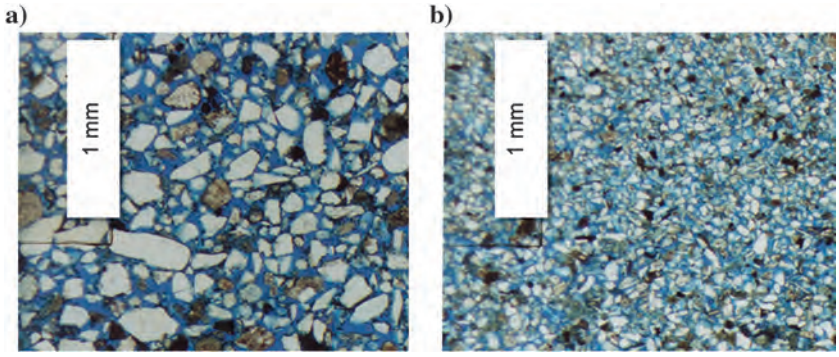

Figure 3. Thin sections describing pore network systems (HRT) formed by different grain sizes. (a) HRT-1 (porosity = 32 p.u., permeability = 852 mD); (b) HRT-3 (porosity = 27 p.u., permeability = 121 mD).

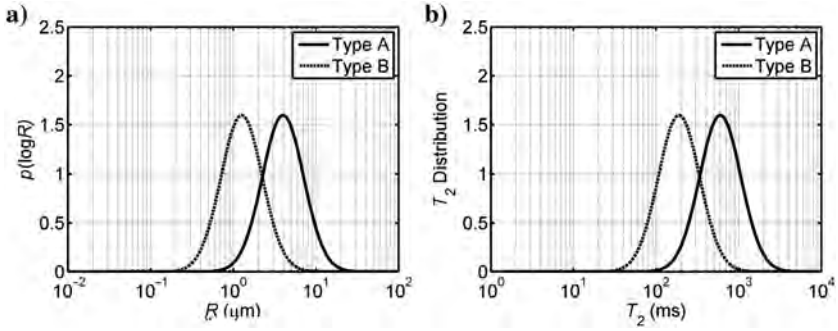

Figure 4. (a) Pore-size distributions, and (b) NMR T_2-distributions of two different rock types exhibiting different grain-size distributions.

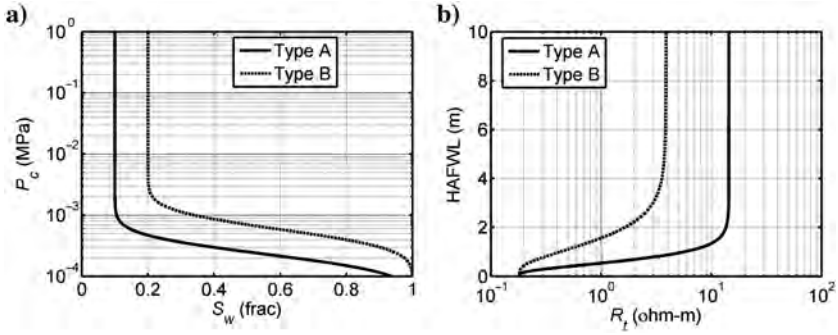

Figure 5. (a) Drainage capillary pressure, and (b) resistivity-height relation of two different rock types. Here, P_c is capillary pressure; HAFWL is height above free water level; and R_t is resistivity.

When Λ is less than 0.1 μm, the electrical conductivity decreases with increasing pore size. The lowest water salinity case ($C_w = 10$ kppm) exhibits the highest sensitivity between electrical conductivity and pore size. When Λ exceeds 0.1 μm, electrical conductivity is only marginally affected by pore size at all water salinity values. On the contrary, hydraulic conductivity is proportional to the square of Λ as indicated in equation 3 (Figure 1b).

In equation 4, the surface conductivity term becomes negligibly small compared to bulk water conductivity when three conditions are met simultaneously: (1) large pore size, Λ; (2) high connate-water salinity; and (3) high water saturation. Figure 2a shows the theoretical calculation of the ratio between surface conductivity term and bulk conductivity terms as a function of characteristic pore size for different values of water salinity. In the large pore-size end ($\Lambda > 0.1$ μm), the ratio is generally below 0.05 for 100% water-saturated rocks. Consequently, HRT of different pore sizes within a similar porosity range cannot be effectively differentiated

Table 1. Grain size scale table (Wentworth, 1922); phi = $-\log_2 D$, where D is grain diameter in millimeters.

Grain type	Diameter D (μm)	Phi scale
Coarse sand	1000–500	0–1
Medium sand	500–250	1–2
Fine sand	250–125	2–3
Very fine sand	125–63	3–4
Coarse silt	63–32	4–5
Medium silt	32–16	5–6
Fine silt	16–8	6–7
Very fine silt	8–4	7–8
Clay	<4	>8

by resistivity logs in a water-bearing zone. Figure 2b shows the theoretical calculation of the ratio between surface conductivity term and bulk conductivity terms as a function of characteristic pore size for different values of water saturation. The contribution of surface conductivity is elevated by decreasing water saturation, but still remains low. In other words, even when different rock types exhibit the same low water saturation (<10%), their electrical conductivity still cannot differentiate them effectively.

Sensitivity of resistivity to HRT in a hydrocarbon-bearing zone

It is noteworthy that the electrical conductivity of a partially saturated rock is greatly sensitive to water saturation, as described in equation 4. If different HRT exhibited different water saturations in a hydrocarbon-bearing zone, resistivity logs would be diagnostic of HRT. To illustrate this point, we use a simple pore-scale model to study the cause-and-effect chain connecting a series of rock properties including grain-size distribution,

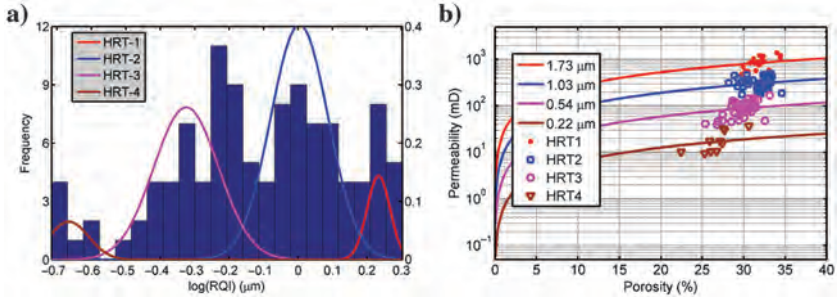

Figure 6. Hydraulic rock typing from the histogram distribution of logarithmic RQI calculated from routine core porosity-permeability measurements. (a) Histogram of logarithmic RQI, and (b) classified HRT on the porosity-permeability plot.

Table 2. Statistical distributions of helium porosity, air permeability (with Klinkenberg correction), and grain-size data (d10, d25, and mean value) from laser particle size analysis for each HRT.

Rock type	Porosity (%)	Permeability (10^3 μm^2)	Grain size d10 (μm)	Grain size d25 (μm)	Mean grain size (μm)
HRT-1	32.1 ± 1.2	973 ± 190	230 ± 32.2	170 ± 28.7	99 ± 25.6
HRT-2	31.6 ± 1.5	340 ± 120	152 ± 14.6	122 ± 11.8	46 ± 5.0
HRT-3	29.6 ± 1.6	88.0 ± 34.5	86 ± 9.2	63 ± 6.5	33.5 ± 3.32
HRT-4	25.9 ± 1.7	13.1 ± 3.67	57 ± 7.8	42 ± 6.2	20.8 ± 4.2

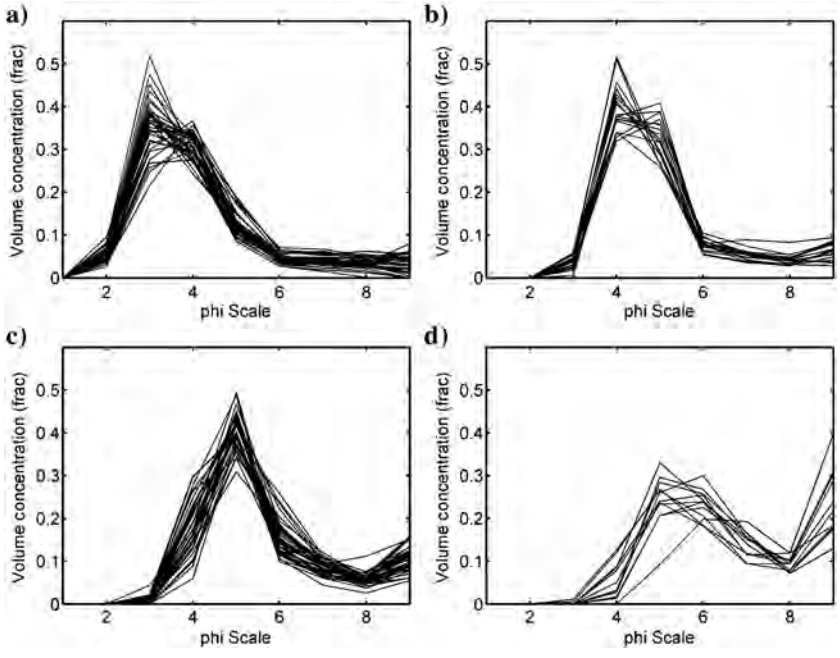

Figure 7. Grain-size distributions measured from laser particle size analyzer for each HRT group: (a) HRT-1; (b) HRT-2; (c) HRT-3; (d) HRT-4.

pore-body size distribution, pore-throat size distribution, capillary pressure, water saturation, NMR transverse relaxation time T_2 distribution, and electrical conductivity. For simplicity, we only compare two ideal rock models: one of large grain size (100 μm) and the other of small grain size (50 μm). Figure 3 shows two thin sections of pore network systems formed by large (Type A) and small grain sizes (Type B), respectively. Log-normal density functions are used to model pore-body size distribution and pore-throat size distribution (Xu and Torres-Verdín, 2013).

NMR transverse relaxation time (T_2) is mainly sensitive to pore-body size. With the assumption that bulk relaxation and diffusion coupling are negligible in a fully water-saturated, water-wetting rock sample measured under a constant magnetic field, T_2 is related to pore-body size by (Coates et al., 1999)

$$\frac{1}{T_2} = \rho \frac{S}{V}, \tag{5}$$

where ρ is surface relaxivity in μm/s, and S/V is surface to volume ratio in μm^{-1} which quantifies pore-body dimension. Large grain sizes generate large pore sizes accordingly, resulting in a large T_2 distribution (Figure 4). Capillary pressure (P_c) relates to pore-throat size through Laplace's equation

$$P_c = \frac{2\Gamma|\cos\theta|}{R_{\text{th}}}, \tag{6}$$

where R_{th} is pore-throat radius in μm, Γ is interfacial tension, and θ is contact angle. With the assumption that pore-throat size is linearly correlated with pore-size, we modeled capillary pressure curves for these two different rock types (Figure 5a). When the two rocks are subject to the same capillary pressure induced by hydrocarbon migration at reservoir conditions, rock type A exhibits lower capillary-bound water saturation and lower clay hydration water saturation (Hill et al., 1979), and consequently lower electrical conductivity (Figure 5b). Therefore, in a hydrocarbon-bearing zone, resistivity logs become sensitive to pore size and are therefore diagnostic of HRT. Rock types with higher hydraulic conductivity tend to exhibit lower electrical conductivity (or higher resistivity) in hydrocarbon-bearing zones and in the presence of high capillary pressure.

Field observations: Marco Polo Field, Gulf of Mexico, USA

The field under study is a Miocene turbidite oil reservoir located in the deepwater Gulf of Mexico (water depth ~1200 m) (Contreras et al., 2006; Xu and Torres-Verdín, 2012). The depositional system is interpreted as a submarine fan complex developed in a minibasin with stacked progradational lobes. Reservoirs primarily consist of sandy turbidite facies interbedded with muddy debris-flow facies. Reservoir rocks are mainly unconsolidated sandstones with very fine to fine to medium-size grains (see Table 1 for grain-size descriptions). Mean pore radii of most reservoir rocks are larger than 0.1 μm. Connate water salinity is approximately 160 kppm of NaCl equivalent.

Core-based hydraulic rock typing

About 100 ft whole core were acquired from the formations to be analyzed. HRT is ranked and classified with the reservoir quality index (RQI) (Leverett, 1941; Amaefule et al., 1993) calculated from routine core porosity-permeability measurements via

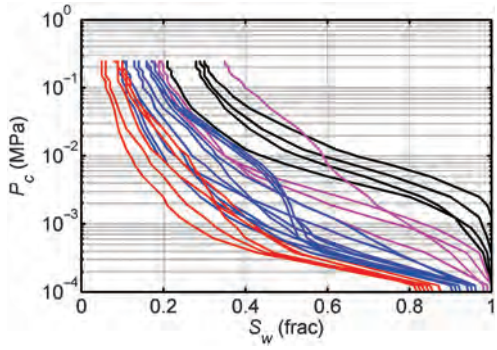

Figure 8. Primary drainage capillary pressure curves modeled from laser particle size analyzer measured grain-size distributions.

Table 3. Grain-size distribution measured with laser particle size analysis for HRT and associated facies interpretation.

Rock type	Grain-size distribution	Description	Facies interpretation
HRT-1	Figure 7a	Dominated by fine and very fine sand grains; unimodal grain-size distribution	Turbidite channel infill including channel lag
HRT-2	Figure 7b	Dominated by very fine sand and coarse silt grains; unimodal grain-size distribution	Turbidite channel levee or margin
HRT-3	Figure 7c	Dominated by coarse and medium silt grains; unimodal grain-size distribution	Turbidite channel levee or margin
HRT-4	Figure 7d	Dominated by fine silt and clay-sized grains; bimodal grain-size distribution	Overbank deposits possibly including thin debris flows

$$\mathrm{RQI} = 0.0314\sqrt{k/\phi}, \quad (7)$$

where k is permeability in mD, ϕ is porosity in fraction, and RQI is in μm. Figure 6a shows the histogram of calculated RQI on a logarithmic scale. A Gaussian mixture clustering algorithm (Press et al., 2007) was applied to logarithmic RQI to separate core samples into four HRT (Figure 6b). Table 2 summarizes the statistics of petrophysical properties associated with each HRT. We observe that neighboring rock types exhibit a largely overlapping porosity range. These four HRT are further verified with laser-particle grain-size measurements (Figure 7) and the corresponding modeled capillary pressure curves (Figure 8). Generally, larger grain sizes originate larger pore sizes that give rise to larger hydraulic conductivity or better HRT. Table 3 establishes a possible correlation between HRT and sedimentary facies. Water saturation measured with Dean-Stark's method in cores acquired with oil-base mud provides validation for the relationship between hydraulic conductivity and water saturation in different rock types (Figure 9).

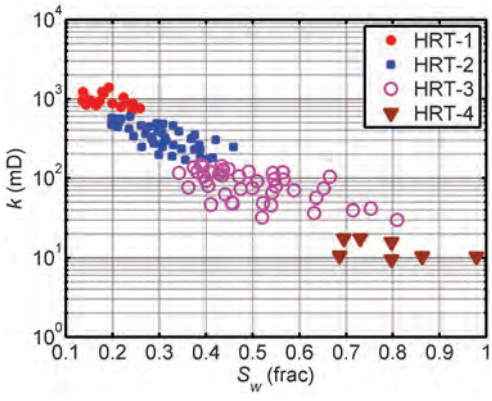

Figure 9. Correlation between core-measured permeability and water saturation for each HRT.

Verification in the water-bearing zone (XY48–XY56 M)

Figure 10 shows a water-saturated interval from the turbidite reservoir. Lithology in this interval is mainly clean sandstone and neighboring rock types have a largely overlapping porosity range as shown in Table 2. Their hydraulic properties are mainly determined by depositional grain sizes. As a result, gamma ray, neutron porosity, bulk density, and resistivity logs do not exhibit significant variability because these logs are not directly sensitive to grain size. The variability of these logs can only differentiate the upper half zone from the lower half zone (Track 8). However, NMR logs including logarithmic-mean T_2 (T2LM), bound fluid volume (BFV), and free fluid volume (CMFF) show good sensitivity to HRT. We use two different workflows to classify rock types by invoking the same k-means clustering algorithm (Press et al., 2007). The first workflow uses NMR logs as input attributes to classify rock types. The second workflow uses resistivity logs as input attributes and invokes the same clustering algorithms to classify rock types. We found that rock classification results obtained with the first workflow (Track 7) exhibit higher resolution and variability than those obtained with the second workflow (Track 8). This simple case indicates that resistivity logs do not contribute as much useful information as NMR logs do for rock typing within a water-bearing zone.

Verification in the oil-bearing zone (XX20–XX35 M)

Figure 11 shows an oil-saturated zone from the turbidite reservoir, which covers essentially the same rock types distributed in the water-bearing zone. Resistivity logs show much larger variability when compared to those acquired within the water-bearing zone. Resistivity logs exhibit a similar pattern to the NMR T2LM log. Moderate to high correlations are observed between the deepest-sensing resistivity log (AHT90) and T2LM and BFV logs (Figure 12). We use two different workflows

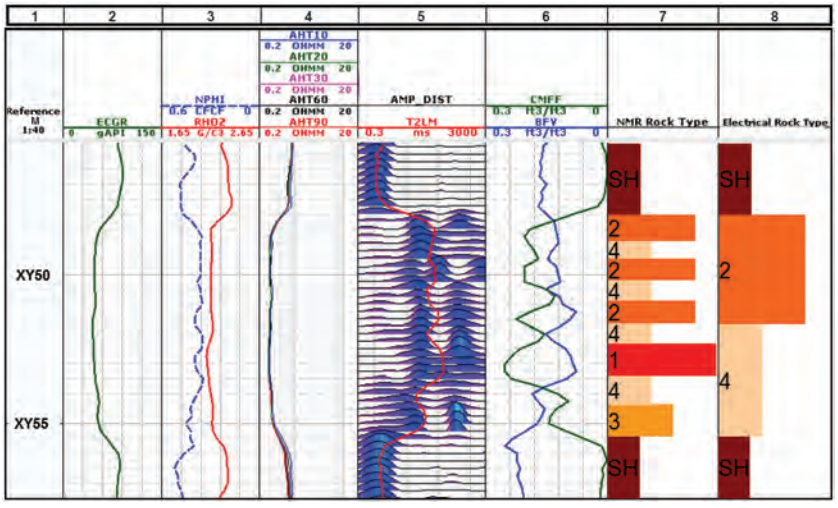

Figure 10. Comparison of resistivity- and NMR-derived rock types in a water-bearing zone. Track 1: Depth; Track 2: Gamma ray log; Track 3: Neutron (in sandstone porosity units) porosity and bulk density logs; Track 4: Induction resistivity logs; Track 5: NMR logs; Track 6: NMR free- and bound-fluid volume logs; Track 7: NMR-derived rock types; Track 8: Resistivity-derived rock types.

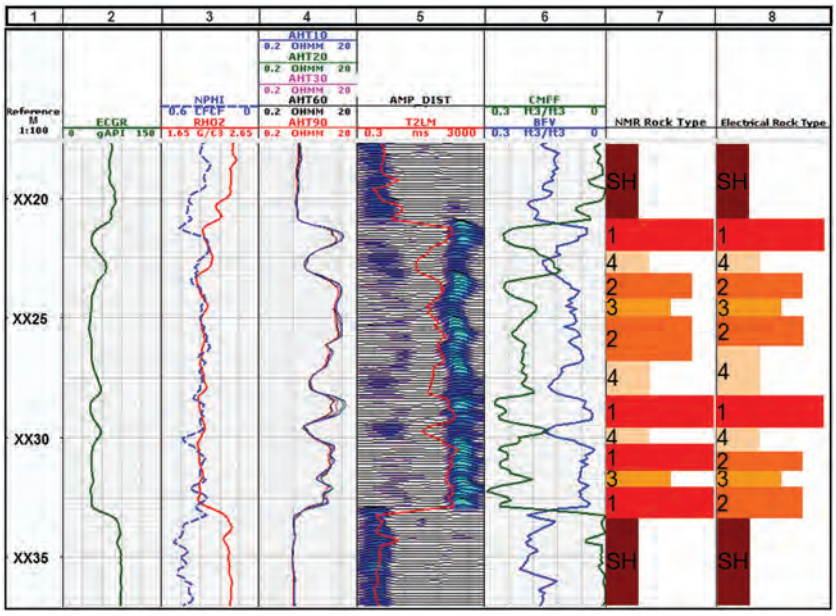

Figure 11. Comparison of resistivity- and NMR-derived rock types in an oil-bearing zone. Track 1: Depth; Track 2: Gamma ray log; Track 3: Neutron porosity (in sandstone porosity units) and bulk density logs; Track 4: Induction resistivity logs; Track 5: NMR logs; Track 6: NMR free- and bound-fluid volume logs; Track 7: NMR-derived rock types; Track 8: Resistivity-derived rock types. The whole core was acquired from a zone that is 300 ft above this oil-bearing zone.

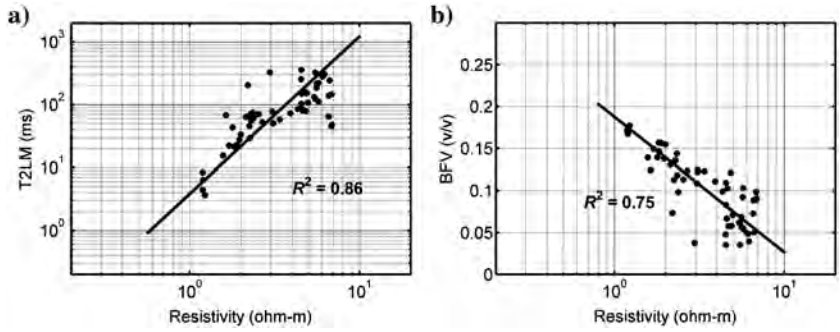

Figure 12. (a) Correlation between resistivity and NMR T2LM logs ($R^2 = 0.86$) in the oil-bearing zone. (b) Correlation between resistivity and NMR BFV logs ($R^2 = 0.75$) in the oil-bearing zone.

to classify rock types invoking the *k*-means clustering algorithm for this oil-bearing interval. The first workflow uses a combination of gamma ray, neutron porosity, bulk density, and NMR logs as input attributes to classify rock types. The second workflow replaces NMR logs with resistivity logs and invokes the same *k*-means clustering algorithms to classify rock types. We found that the classification results obtained with the two workflows agree well (Tracks 7 and 8). This case indicates that resistivity logs are good substitutes for NMR logs when performing log-based rock typing in hydrocarbon-bearing zones at irreducible water saturation.

Limitations

The rock typing workflow that includes resistivity logs has several limitations. First, the resolution of rock typing is limited by the intrinsic vertical resolution of the deep apparent resistivity log, which is approximately 2.5 ft. Rock typing results may be subject to large uncertainty in thinly bedded or laminated zones due to shoulder-bed effects (Xu et al., 2013c). Second, presence of free (mobile) water in the capillary transition zone (Xu and Torres-Verdín, 2012) affects the resistivity logs, resulting in underestimation of rock hydraulic properties without applying appropriate corrections. Third, resistivity logs can be adversely affected by deep mud-filtrate invasion in water-based mud drilled wells. Numerical well log modeling coupled with near-borehole invasion simulation may be necessary to remedy such adverse effects on resistivity logs (Xu et al., 2012).

Conclusions

Pore size has different effects on the electrical and hydraulic conductivity of rocks. In water-bearing zones where capillary pressure is absent, electrical conductivity is only marginally affected by pore size, thereby leading to poor ranking of HRT. In hydrocarbon-bearing zones, different HRT, when subject to reservoir capillary pressure, tend to exhibit different values of water saturation. Rocks with better hydraulic properties exhibit lower capillary-bound water saturation and clay-hydration water saturation, giving rise to lower electrical conductivity. Consequently, resistivity logs become sensitive to HRT in hydrocarbon-bearing zones.

We verified the above interpretations using pore-scale models and field observations from a deep-drilling well penetrating turbidite oil reservoirs in the Gulf of Mexico. The field data test shows that inclusion of resistivity logs in the rock classification workflow can significantly enhance the accuracy of hydraulic rock typing in hydrocarbon-bearing zones which remain at irreducible water saturation conditions.

Acknowledgments

We thank Anadarko Petroleum Corporation for providing the data used in the field studies. The work reported in this paper was funded by The University of Texas at Austin's Research Consortium on Formation Evaluation, jointly sponsored by Afren, Anadarko, Apache, Aramco, Baker-Hughes, BG, BHP Billiton, BP, Chevron, China Oilfield Services, LTD., ConocoPhillips, ENI, ExxonMobil, Halliburton, Hess, Maersk, Marathon Oil Corporation, Mexican Institute for Petroleum, Nexen, ONGC, OXY, Petrobras, PTTEP, Repsol, RWE, Schlumberger, Shell, Statoil, Total, Weatherford, Wintershall, and Woodside Petroleum Limited. A special note of gratitude goes to Yonghe Sun and several anonymous reviewers for their constructive technical and editorial comments that improved the first version of the manuscript.

References

Allen, D., C. Flaum, T. S. Ramakrishnan, J. Bedford, K. Castelijins, D. Fairhurst, G. Gubelin, N. Heaton, C. C. Minh, M. A. Norville, M. R. Seim, T. Pritchard, and R. Ramamoorthy, 2000, Trends in NMR logging: Oilfield review/Schlumberger, **12**, 2–18.

Amaefule, J. O., M. Altunbay, D. Tiab, D. G. Kersey, and D. K. Keelan, 1993, Enhanced reservoir description: Using core and log data to identify hydraulic (flow) units and predict permeability in uncored intervals/wells: SPE Annual Technical Conference and Exhibition, paper SPE 26436, 3–6.

Archie, G. E., 1942, The electrical resistivity log as an aid in determining some reservoir characteristics: Transactions of the AIME, **146**, 54–62.

Asquith, G. B., and C. R. Gibson, 1982, Basic well log analysis for geologists, 1st ed.: AAPG.

Bolève, A., A. Crespy, A. Revil, F. Janod, and J. L. Mattiuzzo, 2007, Streaming potentials of granular media: Influence of the Dukhin and Reynolds numbers: Journal of Geophysical Research, **112**, B08204, doi: 10.1029/2006JB004673.

Coates, G. R., L. Xiao, and M.G. Prammer, 1999, NMR logging principles and application, Halliburton Energy Services: Gulf Publishing Company.

Contreras, A., C. Torres-Verdín, W. Chesters, K. Kvien, and T. Fasnacht, 2006, Extrapolation of flow units away from wells with 3D pre-stack seismic amplitude data: Field example: Petrophysics, **47**, 223–238.

Detmer, M. D., 1995, Permeability, porosity, and grain-size distribution of selected Pliocene and Quaternary sediments in the Albuquerque basin: New Mexico Geology, **17**, 79–87.

Evans, J., C. Cade, and S. Bryant, 1997, A geological approach to permeability prediction in clastic reservoirs, *in* J. A. Kupecz, J. Gluyas, and S. Bloch, eds., Reservoir quality prediction in sandstones and carbonates: AAPG Memoir **69**, 91–101.

Hill, H. J., O. J. Shirley, and G. E. Klein, 1979, Bound water in shaly sands — Its relation to Qv and other formation parameters: The Log Analyst, **20**, no. 3, 3–19.

Johnson, D. L., J. Koplik, and L. M. Schwartz, 1986b, New pore-size parameter characterizing transport in porous media: Physical Review Letters, **57**, 2564–2567.

Johnson, D. L., T. J. Plona, and H. Kojima, 1986a, *in* R. Jayanth, J. Banavar, and K. W. Winkler, eds., Probing porous media with 1st sound, 2nd sound, 4th sound and 3rd sound, in physics and chemistry of porous media, **2**, 243–277: AIP.

Leverett, M. C., 1941, Capillary behavior in porous solids: Transactions of the AIME, **142**, 159–172.

Press, W. H., S. A. Teukolsky, W. T. Vetterling, and B. P. Flannery, 2007, Section 16.1: Gaussian mixture models and k-means clustering, numerical recipes: The art of scientific computing, 3rd ed.: Cambridge University Press.

Pride, S., 1994, Governing equations for the coupled electromagnetics and acoustics of porous media: Physical Review B, **50**, 15678–15696.

Revil, A., 2013, Effective conductivity and permittivity of unsaturated porous materials in the frequency range 1 mHz–1 GHz: Water Resources Research, **49**, 306–327, doi: 10.1029/2012WR012700.

Revil, A., and L. M. Cathles, 1999, Permeability of shaly sands: Water Resources Research, **35**, 651–662.

Revil, A., and P. W. J. Glover, 1998, Nature of surface electrical conductivity in natural sands, sandstones, and clays: Geophysical Research Letters, **25**, 691–694.

Revil, A., and P. Leroy, 2001, Hydroelectric coupling in a clayey material: Geophysical Research Letters, **28**, 1643–1646, doi: 10.1029/2000GL012268.

Schlumberger, 2006, Fundamentals of formation testing: Schlumberger.

Walsh, J. B., and W. F. Brace, 1984, The effect of pressure on porosity and the transport properties of rock: Journal of Geophysical Research, **89**, 9425–9431.

Wentworth, C. K., 1922, A scale of grade and class terms for clastic sediments: Journal of Geology, **30**, 377–392.

Wildenschild, D., J. J. Roberts, and E. D. Carlberg, 2000, On the relationship between microstructure and electrical and hydraulic properties of sand-clay mixtures: Geophysical Research Letters, **27**, 3085–3088, doi: 10.1029/2000GL011553.

Xu, C., Z. Heidari, and C. Torres-Verdín, 2012, Rock classification in carbonate reservoirs based on static and

dynamic petrophysical properties estimated from conventional well logs: SPE Annual Technical Conference and Exhibition, SPE 159991.

Xu, C., and C. Torres-Verdín, 2012, Saturation-height and invasion consistent hydraulic rock typing using multi-well conventional logs: SPWLA 53rd Annual Logging Symposium, paper KK.

Xu, C., and C. Torres-Verdín, 2013, Pore system characterization and petrophysical rock classification using a bimodal Gaussian density function: Mathematical Geosciences, **45**, 753–771, doi: 10.1007/s11004-013-9473-2.

Xu, C., C. Torres-Verdín, and R. J. Steel, 2013b, Geological attributes from well logs: Relating rock types to depositional facies in deepwater turbidite reservoirs: SPE Annual Technical Conference and Exhibition, paper 166178.

Xu, C., C. Torres-Verdín, Q. Yang, and E. Diniz-Ferreira, 2013a, Water saturation — Irreducible or not? The key to reliable hydraulic rock typing in reservoirs straddling multiple capillary windows: SPE Annual Technical Conference and Exhibition, paper 166082.

Xu, C., Q. Yang, and C. Torres-Verdín, 2013c, Bayesian hypothesis testing: Integrating fast well-log forward modeling to validate petrophysical rock typing and to quantify uncertainty in deepwater reservoirs: SPWLA 54th Annual Logging Symposium.

Chicheng Xu received a B.S. (2002) in physics from the University of Science and Techology of China, an MPHIL (2004) in physics from the Chinese University of Hong Kong, and a Ph.D. (2013) in petroleum engineering from the University of Texas at Austin. Before joining the Formation Evaluation Research Consortium group in the Department of Petroleum and Geosystems Engineering at the University of Texas at Austin, he worked at Schlumberger Beijing Geoscience Center as a software engineer from 2004 to 2009. He has published more than 10 technical papers in conferences and journals.

Carlos Torres-Verdín received a Ph.D. (1991) in engineering geoscience from the University of California at Berkeley. During 1991–1997, he held the position of research scientist with Schlumberger-Doll Research. From 1997 to 1999, he was reservoir specialist and technology champion with YPF (Buenos Aires, Argentina). Since 1999, he has been with the Department of Petroleum and Geosystems Engineering of the University of Texas at Austin, where he currently holds the position of Zarrow Centennial Professor. He conducts research on borehole geophysics, formation evaluation, well logging, and integrated reservoir characterization. He is the founder and director of the Joint Industry Consortium on Formation Evaluation at the University of Texas at Austin. He is an Associate Editor for the Borehole Geophysics & Rock Properties section in GEOPHYSICS.

Shuang Gao received a Master's (2004) degree in electronic engineering from Tsinghua University, Beijing, China. From 2004 to 2010, she worked at Schlumberger Beijing Geoscience Center on pressure transient test analysis, well test interpretation, reservoir characterization, and uncertainty analysis. She started a Master's degree in petroleum engineering in The University of Texas at Austin on formation evaluation in 2011. Her research focuses on simulation and interpretation of NMR measurements and organic shale modeling.